European Polymer Journal 152 (2021) 110474

Contents lists available at ScienceDirect

European Polymer Journal

journal homepage: www.elsevier.com/locate/europolj

Preparation of hypercrosslinked PolyHIPEs by using a bio-derived monomer

Burcu Kekevi [a,*], E. Hilal Mert [b,*]

[a] Yalova University, Yalova Community College, Material and Material Processing Department, 77100 Yalova, Turkey
[b] Yalova University, Faculty of Engineering, Department of Polymer Materials Engineering, 77200 Yalova, Turkey

ARTICLE INFO

Keywords:
β-Myrcene
Hypercrosslinking
Friedel-Crafts alkylation
Emulsion templating
PolyHIPE

ABSTRACT

The interest on adapting bio-derived species to polymer synthesis has been increased in the last decade. Terpenes that can be obtained by extracting from the essential oils of tree sap and citrus fruit have an important place on this subject. In this respect, β-myrcene, which is a promising linear conjugated diene, is attracting the interest of researchers. However, the free radical copolymerization of β-myrcene is difficult mainly because of concurrent Diels-Alder reactions with electron-deficient vinyl monomers via their s-cis forms. Here, we developed polyHIPEs from the high internal phase emulsions (HIPEs) of β-myrcene. For this purpose, HIPEs were prepared by using either 50 or 40 vol% of β-myrcene in the continuous phase. Meanwhile, the influence of 4-vinylbenzyl chloride (VBC), divinylbenzene (DVB), and 1,3-butanedioldiacrylate (BDDA) on the copolymerization crosslinking of β-myrcene within precursor HIPEs was explored. For this purpose, HIPEs were prepared by altering the amount of comonomers between 0 and 60 vol% of the total monomer composition. The resulting HIPEs showed excellent stability. However, crosslinking could not be achieved in all cases, due to the altered monomer composition. On the other hand, crosslinked polyHIPEs were hypercrosslinked with Friedel-Crafts alkylation method. Characterization of the resulting materials showed the Brunauer-Emmett-Teller specific surface area (δ_{BET}) of the polyHIPEs was increased from 2.25 $m^2\ g^{-1}$ to 60.18 $m^2\ g^{-1}$ by hypercrosslinking.

1. Introduction

Hierarchical porous structure and high surface area are the important features that make polymers important candidates for the applications such as adsorption [1,2], catalysis [3,4] and energy storage [5,6]. In this context, as being the most convenient approach for the control of the porosity, emulsion templating stands out among the other methods used of creation porosity [7]. The principle of emulsion templating is based on using a concentrated emulsion for the creation of hierarchically ordered porous structure. For this purpose, high internal phase emulsions (HIPEs), which are defined as the emulsions having an internal phase volume fraction (Ø) >0.74, are usually used. In this definition 0.74 is not a random figure, but it is describing the lowest volume fraction at above which the dispersed phase droplets deformed into polyhedra and separated from each other by continuous phase films [8]. When HIPEs are prepared to contain monomeric species in the continuous phase, polymerization of HIPEs leads to the formation of macroporous polymer foams. These foams are known as polyHIPEs [7–9].

PolyHIPEs have unique morphology composed of macropores (or cavities) that are connected to each other by small pore throats. This open-cell structure is known to be the reflection of the used HIPE templates [9,10]. Thereby, controlling the experimental parameters (i.e. surfactant amount, crosslinker ratio, stirring rate, and etc.) during the emulsification step is used as a tool for obtaining well-defined porosity, and as well as improving physical properties [10,11]. Although highly open and hierarchical porous structure offers many advantageous for various applications, dominance of macropores and lack of meso- and micropores in the morphology usually resulted in low specific surface areas changing in the range of 3–20 m^2g^{-1} [12]. The application areas of polyHIPEs can be expanded by changing the porosity scale from macro (>50 nm) to micro (<2 nm) sizes. In this respect, while increasing the crosslinking ratio or using a porogen are effective approaches for extending the specific surface area [12], hypercrosslinking usually provides the advantage of preparing ultrahigh surface area materials [13,14].

Hypercrosslinking of polystyrene networks which was first reported by Davankov and Tsyurupa [15] have been using as an efficient methodology for integrating micropores into polymer networks without

* Corresponding authors.
E-mail addresses: bkekevi@yalova.edu.tr (B. Kekevi), hmert@yalova.edu.tr (E.H. Mert).

https://doi.org/10.1016/j.eurpolymj.2021.110474
Received 16 February 2021; Received in revised form 14 April 2021; Accepted 22 April 2021
Available online 27 April 2021

differentiating the mechanical structure of the matrix. In hypercrosslinking, firstly the polymer is swelled in a suitable polar solvent so that the distance between polymer chains widened. Afterwards, vinyl benzyl chloride (VBC) and its moieties are used as an internal electrophile in the presence of $FeCl_3$ catalyst, and metyhlene bridges are created between the long polymer chains in semi-solution state [13,14–17]. Meanwhile, the collapse of the polymer network during drying and extraction is prevented by the created additional crosslinks. Consequently, a polymer network exhibiting an extensive microporosity is obtained in the dry state [18,19]. Thereby, hypercrosslinking is also a good tool to include micro- and mesopores in the polyHIPE morphology. In fact, reactive sites of a polyHIPE can be developed by hypercrosslinking without changing the material morphology prominently. Moreover, hypercrosslinked polyHIPEs can be used as precursor of carbonized foams [20]. In this respect, Macintyre et al. [21] synthesized poly[divinylbenzene (DVB)-*co*-vinylbenzyl chloride (VBC)] hypercrosslinked materials by using a chloromethyl substituent as an internal electrophile and obtained materials with specific surface areas as high as 1200 m^2g^{-1}. In another study, Woodward et al. [22] synthesized hypercrosslinked poly[styrene (ST)-*co*-divinylbenzene (DVB)] polyHIPEs by using dimethoxymethane as an external crosslinker to "knit" phenyl groups in the polymer network with Friedel-Crafts alkylation method. With this approach specific surface area of the resulting materials was increased up to 417 m^2g^{-1}.

Styrene has been so far the mostly used monomer for polyHIPE synthesis due to its hydrophobicity, easy accessibility, reactivity and cost advantage. Several monomeric kinds including methacrylates [23–25], acrylates [26], dicyclopentadiene [27], ε-caprolactone [28], thiols [29,30], and even resins such as unsaturated polyester [31,32], and epoxy [33], and tannin [34] have been also used in years. However, adaptation of bio-derived and renewable sources in polyHIPEs preparation is also attracting interest of scientists as a result of the increasing demand on environmentally friendly processes, and depletion of petroleum resources. In this context, terpenes have an important place in the synthesis of bio-derived polymers.

Terpenes are specific kinds obtained by extracting from the essential oils of tree sap and citrus fruit. As well as their main applications are in the field of fragrances, cosmetics, pharmaceuticals and food industry, they are also attracting considerable interest in polymer synthesis because of their convenient chemical structure [35]. Terpenes can be polymerized through their double bonds to produce polymer resins. Particularly, *β*-myrcene that has a similar chemical structure with petroleum derived unsaturated hydrocarbons with its three double bonds gives polyisoprene like chains by polymerization [36]. Polymyrcene chains that are exhibiting unsaturation allow further functionalization reactions [37]. On the other hand, as being a linear conjugated diene, *β*-myrcene undergoes concurrent Diels-Alder reactions with electron-deficient vinyl monomers via their cis forms during radical copolymerization [38]. Moreover, its high monomer reactivity and highly hydrophobic nature might prevent the formation of *β*-myrcene based high molecular weight or highly crosslinked copolymers [38].

In our previous work, for the first time in the literature, we reported copolymerization of *β*-myrcene in water-in-oil (w/o) type HIPEs to develop polyHIPEs by using a bio-derived monomeric kind [39]. For this purpose, we used several kinds of comonomers including styrene, DVB, acrylates and methacrylates to achieve highly crosslinked polyHIPE foams based on *β*-myrcene. By this study, we demonstrated the importance of using a comonomer with a spacer group, and the monomer ratio in the continuous phase to obtain a highly crosslinked solid polymer foam exhibiting the desired hierarchical morphology.

Herein, synthesis of hypercrosslinked polymyrcene foams by HIPE templating approach is described. For this aim, polyHIPEs were first synthesized from precursor HIPEs which were obtained by altering the monomer composition in the continuous phase. Thus, 13 different HIPE formulations were prepared. In the experiments the amount of *β*-myrcene was either 50 or 40 vol% of the monomer composition, while the amounts of the comonomers were altered between 0 and 60 vol%. Accordingly, the influence of comonomers on the copolymerization crosslinking of *β*-myrcene within precursor HIPEs was explored. Thereafter, polyHIPE foams produced from the precursor HIPE templates were hypercrosslinked (HXL) in the presence of a Lewis catalyst ($FeCl_3$) via Friedel-Crafts alkylation. Chemical structure, pore morphology and Brunauer-Emmett-Teller (BET) specific surface area (δ_{BET}) of the resulting polyHIPEs and HXL-polyHIPEs were investigated. Thus, the effect of monomer composition on final material properties was demonstrated.

2. Experimental

2.1. Materials

β-Myrcene (technical grade, Sigma-Aldrich), 1,3- butanediol diacrylate (BDDA; 98%, Sigma-Aldrich), poly(ethylene glycol)-*block*-poly (propylene glycol)-*block*-poly(ethylene glycol) (Pluronic® L-121; Mn ~ 4400, non-ionic surfactant, Sigma-Aldrich), sorbitane monooleate (Span® 80, non-ionic surfactant, Sigma-Aldrich), potassium persulfate (KPS; ≥99.0%, ACS reagent), calcium chloride hexahydrate ($CaCl_2{\cdot}6H_2O$; 98%, Sigma-Aldrich), $FeCl_3$ (anhydrous, powder, ≥99.99% trace metals basis, Sigma-Aldrich), 1,2-dichloroethane (DCE, ≥99.0%, ACS reagent), tetrahydrofuran (THF, ≥99.9%, Sigma-Aldrich) were used as received. In all experiments ultrapure double distilled deionized water was used.

2.2. Synthesis of terpene-based polyHIPEs

Terpene-based polyHIPEs were synthesized with 80 vol% of nominal porosity. While the ratio of *β*-myrcene in the continuous phase corresponds to 50 or 40 vol%, the ratio of comonomers was changed between 0 and 60 vol% of the monomer composition. With this approach 13 different HIPE formulations were obtained. Monomer compositions of the HIPEs are presented in Table 1. In Table 1, HIPEs were named as HIPE-x, where x is designating the experiment number.

In a classical experiment, *β*-myrcene, comonomers and surfactants (Pluronic® L 121 and Span® 80) were added into a round-bottom two-necked glass reactor which was equipped with an overhead stirrer and a peristaltic pump. In the formulations the total amount of the surfactants was equal to the 30 vol% of the continuous phase, and each surfactant has equal volume proportions. Once all components were added into the reactor, continuous phase was stirred for 10 min to obtain a homogeneous mixture. Afterwards, aqueous phase containing 1 wt% of $CaCl_2{\cdot}6H_2O$ (regarding to aqueous phase) and KPS (1 mol %, regarding to monomer composition) was added by droplets with the help of a peristaltic pump, under constant stirring (@400 rpm). When the addition of aqueous phase completed stirring was continued for an extra 30 min to obtain a homogeneous emulsion. Then, obtained HIPE was transferred into a glass container and placed in an air-circulating

Table 1
Monomer composition of HIPEs.

HIPE	*β*-Myrcene (vol. %)	BDDA (vol. %)	DVB (vol. %)	VBC (vol. %)
HIPE-1	50	30	10	10
HIPE-2	50	20	10	20
HIPE-3	50	10	10	30
HIPE-4	50	–	25	25
HIPE-5	50	–	20	30
HIPE-6	50	–	15	35
HIPE-7	50	–	10	40
HIPE-8	50	10	–	40
HIPE-9	50	50	–	–
HIPE-10	50	–	50	–
HIPE-11	50	–	–	50
HIPE-12	40	–	60	
HIPE-13	40	–	–	60

constant temperature oven at 60 °C and kept for 24 h to achieve crosslinking. Afterwards, crosslinked foam was removed from the glass container and extracted with ethanol in a Soxhlet apparatus for 24 h. Finally, polyHIPE foam was dried under vacuum at 40 °C until the constant weighing is available.

In the end, 5 different solid polyHIPE foams were produced from the precursor HIPEs. Resulting polyHIPEs were labelled as MBx, where x is the number of HIPE formulation.

2.3. Hypercrosslinking of polyHIPEs

Hypercrosslinking of resulting polyHIPEs was achieved by using post-polymerization hypercrosslinking method which is based on Friedel-Crafts alkylation reaction [40]. For this purpose, ~2.5 g of powdered polyHIPE sample was put into 50 mL of 1,2-dichloroethane (DCE) and left to swollen for 2 h in a round-bottom glass reactor equipped with a thermometer. Then the reactor was placed in an ice bath and when the temperature was decreased to 4 °C, 2.5 g of $FeCl_3$ was added into the reactor under constant stirring (300 rpm). Thereafter, the reactor was placed in an oil bath on a magnetic stirrer and the temperature was increased up to 80 °C and the reaction was continued for 18 h to achieve conversion of reactive groups to methylene bridges to obtain hypercrosslinked (HXL) structure. In the end, HXL-polyHIPEs were removed from the reaction mixture by filtration and rinsed with 1% (v/v) of aqueous hydrochloric acid solution and then deionized water. Finally, HXL-polyHIPEs were extracted with ethanol for 24 h and dried under vacuum at 40 °C, until constant weighing is available [40,41]. HXL-polyHIPEs were labelled as HMBx, where x is the formulation number of the HIPE template used for polyHIPE synthesis.

In order to reveal the influence of atmospheric conditions on hypercrosslinking reaction, HXL-polyHIPEs were prepared under Argon atmosphere. In these experiments all the reaction conditions were identical with the procedure described above. The only difference was that Argon gas was passed through the reactor before hypercrosslinking and continued during the hypercrosslinking reaction process. To distinguish the composition of the HIPEs, resulting materials synthesized under inert conditions were labelled as IHMBx, where x is designating the number of HIPE formulation.

2.4. Solubility test

Crosslinking of HIPEs was investigated by a simple solubility test. For this purpose, ~0.3 g of polyHIPE sample was immersed in 20 mL of tetrahydrofuran (THF) and stirred at 25 °C for 24 h. Afterwards, polyHIPE sample was filtered, extracted with ethanol and dried under vacuum at 40 °C until constant weighing is available. Then the loss of mass was calculated to determine the amount of soluble polymer in the resulting polymer network.

2.5. Characterization

Chemical structures of the polyHIPEs and HXL-polyHIPEs were confirmed by Fourier transform infrared (FTIR) spectroscopy. For this purpose, spectrums of the monomers and the obtained polyHIPEs were all recorded on a Perkin Elmer Spectrum 100 Fourier transform infrared spectrometer in 500–4000 cm^{-1}.

Additionally, Nuclear Magnetic Resonance (NMR) spectroscopy was used to confirm the chemical structures of obtained materials. For this purpose, a JEOL ECZ500 model instrument was used. While the ^1H NMR of β-myrcene was recorded in the liquid state by using $CDCl_3$, ^1H NMR spectrums of the polyHIPE and HXL-polyHIPE samples were recorded in the solid-state.

The investigation of the morphology of polyHIPEs was performed by Scanning Electron Microscopy (SEM; ZEISS Supra 40 VP, Germany). For this aim, polyHIPE samples were first coated with gold. By using the taken SEM images, average cavity size (CS) and interconnected pore size (IPS) of each sample was calculated. For the calculation of CS, the diameter of over 100 cavities was taken, whereas IPS was calculated by taking over 150 measurements. Before calculating the statistical average and error, each measurement was multiplied with a correction factor ($2/3^{1/2}$) [42].

Brunauer-Emmett-Teller (BET) specific surface area (δ_{BET}) of the polyHIPEs was measured by using Micromeritics Gemini VII Surface Area and Porosity Analyzer (Micromeritics Instrument Corporation, USA). All the measurements were performed after degassing which was conducted at 100 °C for 24 h, under nitrogen flow on a degassing unit (Micromeritics FlowPrep 060 Sample Degas Unit, Micromeritics Instrument Corporation, USA). δ_{BET} of the polyHIPEs was calculated by applying BET equation on the recorded N_2 adsorption/desorption isotherms. For each polyHIPE sample, δ_{BET} was calculated from the arithmetic average of 3 different measurement conducted by using 3 different specimens.

Mechanical properties of the resulting polyHIPEs were investigated according to the ASTM D1621-2004 standard test method by using Zwick Universal Testing Machine (Zwick GmbH&Co.KG, Germany). Compressive stress/strain plots were recorded by applying 10 kN of uniaxial compressive load on intact polyHIPE foams without applying any cutting or breaking to the samples. 3 identical specimens were tested for each polyHIPE sample and elastic modulus was determined from the stress/strain plots of the samples by using the original software of the testing machine. The elastic modulus was calculated from the arithmetic averages of the elastic modulus of 3 identical specimens for each polyHIPE sample.

3. Results and discussion

Herein, in order to develop novel polyHIPE materials we created formulations composed of β-myrcene, BDDA, VBC and DVB. Since β-myrcene provides isoprene like structure and BDDA also contributes on chain flexibility one of the goals in here was to diminish the brittleness arises from porous structure and rigid monomeric units. Since it is a sustainable monomer, we intended to keep the amount of β-myrcene in the continuous phase at least 50 vol% of the total monomer composition. We also intended to provide suitable sites for post-polymerization hypercrosslinking reactions. In this respect, the amounts of DVB and VBC in the HIPE formulations were altered considering that DVB plays an important role in creating suitable crosslinking points and VBC forms a hypercrosslinked network by providing interconnections with methylene bridges between aromatic rings [43]. HIPEs were prepared by varying the ratio of DVB and VBC between 0 vol% and 60 vol% of the total monomer composition.

However, it is known from the previous studies that synthesis of high molecular weight polymers from β-myrcene by free radical polymerization or copolymerization is often restricted due to the linear conjugated diene structure [44–46]. We know based on the results of our previous study that using comonomers having long spacer groups during copolymerization reactions of β-myrcene facilitate the formation of crosslinked polymer matrices [39]. Thereby, BDDA comonomer was not only used to increase the chain flexibility but also to achieve the preparation of crosslinked polymer networks by copolymerization of β-myrcene in HIPE templates. Since, this is the first time of using this monomer composition in polyHIPE synthesis, the influence of monomer mixture on the stability and crosslinking performance of HIPEs was investigated. Emulsion stability is a crucial parameter for polyHIPEs, because cavities of a polyHIPE reflect the droplets of precursor HIPEs. If the two major destabilization processes, Ostwald ripening and coalescence cannot be prevented they lead the droplets merge and form larger ones [47,48]. This would result in the creation of larger cavities in the polyHIPE morphology. In addition, cavity size distribution would also expand [49]. On the other hand, it is also important that the emulsion stability is maintained until the gel point is reached during polymerization [10].

Emulsion stability of the prepared HIPEs was explored by observing phase separation behaviours at two different temperatures. For this purpose, two sets of HIPEs were prepared by using the monomer compositions given in Table 1. However, internal phases were prepared without polymerization initiator (KPS). Once HIPEs were obtained they transferred into sealed glass containers. Then the first set was placed in a constant temperature oven at 25 °C, while the second set was placed in another oven at 60 °C. Then it was checked whether there was phase separation on a daily basis. These temperatures were selected based on the conditions that HIPEs are prepared and polymerized. It was observed that each HIPE formulation exhibited phase integrity more than 30 days at 25 °C, and more than 24 h at 60 °C. Since polymerization of a HIPE is usually completed within 24 h, these results show that the necessary stability criterion is provided. The stability behaviour of the obtained HIPEs is presented in Table 2 accompanying with the crosslinking performance of each HIPE. After it was determined that HIPEs did not exhibit phase separation at 60 °C within 24 h, the same formulations were used as precursors for polyHIPEs. For this purpose, another set of HIPE was prepared with the monomer compositions presented in Table 1, this time by using KPS in the aqueous phase. Then the precursor HIPEs were placed in an air circulating oven at 60 °C and left in the oven for 24 h for the completion of crosslinking. At the end of 24 h it was observed that only HIPE-1, HIPE-2, HIPE-3, HIPE-4 and HIPE-9 yielded crosslinked solid polyHIPE foams (MB1, MB2, MB3, MB4, and MB9). Crosslinked foams were tested for solubility after purification. However, no significant loss of mass was detected. On the other hand, it was also observed that precursor HIPEs (HIPE-x formulations; x = 5, 6, 7, 8, 10, 11, 12 and 13) which did not yield solid polyHIPE foams were like gel creams and they were all preserving their phase integrity.

This result might be attributed to the regioselectivity and high monomer reactivity of *β*-myrcene. *β*-Myrcene has four regioregular microstructures including *1,4-cis*, *1,4-trans*, *3,4* and *1,2* structures. According to Bauer et al, regioselectivity is higher at low temperatures as compared to polymerizations carried out at high temperatures [50]. Depending on the polymerization conditions of the precursor HIPEs, it is possible for more than one regioregular microstructure to form during polymerization [50–52]. Conjugated double bonds of *β*-myrcene might also cause steric hindrance in copolymerization reactions. In these cases, the growth of polymer chain radicals might be limited, or crosslinking might be prevented.

On the other hand, since *β*-myrcene has high reactivity, it might tend to add its own monomer to the growing chains in free radical copolymerization reactions. Accordingly, it might be difficult to obtain copolymers exhibiting the preferred microstructure [44–46,50]. In free radical copolymerization, microstructure of the copolymer chains is highly dependent on monomer reactivities. Since different monomers form different radical structures, with the relative rates of chain growth dependent on the structure of both monomer and radical. On the other hand, reactivity ratios also control copolymer sequence distribution along the chain. However, reactivity of a monomer in copolymerization reactions cannot be predicted based on its reactivity in homopolymerization and reactivity of the comonomer(s) should also be considered [53]. The effects of monomer composition and reactivity ratios on copolymerization crosslinking of *β*-myrcene based HIPEs can be understood more clearly by evaluating the crosslinking performances of HIPE-9, 10, 11, 12 and 13. As can be seen from Table 2, solid polyHIPE foams could not be obtained from copolymerization of HIPEs prepared using equal volume proportions of *β*-myrcene and DVB or *β*-myrcene and VBC in the continuous phase composition (HIPE-10 and HIPE-11). Lowering the volume ratio of *β*-myrcene in the monomer composition to 40% and increasing the ratio of DVB or VBC to 60% at the same time (HIPE-12 and HIPE-13) were also not resulted with crosslinked polyHIPEs. On the other hand, HIPEs prepared using equal volume proportions of *β*-myrcene and BDDA resulted in polyHIPE material (MB9). This result can be explained by the reduction of steric hindrance and the increase of the degree of crosslinking with the contribution of flexible comonomer units. It might also be explained by the high reactivity of BDDA in the copolymerization reaction with myrcene. On the other hand, it is consistent with our previous results [39].

Table 2
Stability and crosslinking behaviours of HIPEs.

HIPE	Stability @25 °C	Stability @60 °C	Crosslinked Foam
HIPE-1	>1 month	>24 h	Yes
HIPE-2	>1 month	>24 h	Yes
HIPE-3	>1 month	>24 h	Yes
HIPE-4	>1 month	>24 h	Yes
HIPE-5	>1 month	>24 h	No
HIPE-6	>1 month	>24 h	No
HIPE-7	>1 month	>24 h	No
HIPE-8	>1 month	>24 h	No
HIPE-9	>1 month	>24 h	Yes
HIPE-10	>1 month	>24 h	No
HIPE-11	>1 month	>24 h	No
HIPE-12	>1 month	>24 h	No
HIPE-13	>1 month	>24 h	No

In order to review the influence of monomer composition on the pore morphology SEM imagining was used, and SEM images of MB1, MB2, MB3 and MB4 samples are presented in Fig. 1, while the SEM image of MB9 is presented in the *Supplementary Information File* (*see Fig. S1* in the *SI* document). On the other hand, average cavity sizes (CS) and interconnected pore sizes (IPS) were given in Table 3. According to the SEM images given in Fig. 1 and Fig. S1, MBx foams are all exhibiting the well-known polyHIPE morphology composed of large cavities and interconnected pores. On the other hand, Table 3 reveals the significant influence of monomer composition on the pore size. It was determined from Table 3 that the foams MB1, MB2, MB3 and MB4 had larger cavities and interconnected pores when the BDDA amount increased and VBC amount decreased in the formulation. When the average cavity size of MB1 and MB2 samples were compared, it was found that the cavity size decreased from 6.51 μm to 4.15, when the VBC ratio was increased by 10 vol% and the BDDA ratio was decreased by the same amount. It was also determined that decreasing the amount of BDDA by 10 vol% and increasing the amount of VBC by 30 vol% increased the average cavity size up to 7.14 μm. This change observed in cavity dimensions depending on the monomer composition was also observed for interconnected pores. Accordingly, it was determined that the interconnected pore size of the foams MB1, MB2, MB3 and MB4 increased from 0.61 μm to 1.48 μm with the change in the amount of BDDA and VBC in HIPE formulations. On the other hand, MB9 foam was found to have smaller cavities (1.87 μm) and pore connections (0.12 μm) (Table 3). Since the cavities of a polyHIPE is reflecting the droplets of precursor emulsions [10,11], the decrease in the average cavity size can be attributed to the increased emulsion stability. Because the surface energy per unit area is lower in more stable emulsions, droplet size is decreased [49]. On the other hand, in case of *β*-myrcene based polyHIPEs, the variation of cavity size can also be explained by the change of the amount of BDDA. Because crosslinking of *β*-myrcene can be easily achieved with the presence of comonomers with long spacer groups [39,44,46], the other reason of the increase in cavity size might be the low crosslinking ratio [54]. Hence, it is also not an unexpected result MB4 has the larger cavities, while MB9 has the smaller ones.

The BET specific surface area (δ_{BET}) of the MBx samples were measured by applying BET equation to their N_2 adsorption/desorption isotherms, and the obtained data are also presented in Table 3. It was determined that the specific surface area of the MB1, MB2, MB3 and MB4 foams was decreased from 5.79 m^2g^{-1} to 2.25 m^2g^{-1}, when the volume ratio of BDDA comonomer in HIPE formulations was decreased from 30% to 0%. It is also not unexpected that the BET specific surface area for MB9 foam increases to 36.12 m^2g^{-1} due to the variation of cavity dimensions.

The influence of monomer composition on the final material properties was also investigated in terms of mechanical properties. For this

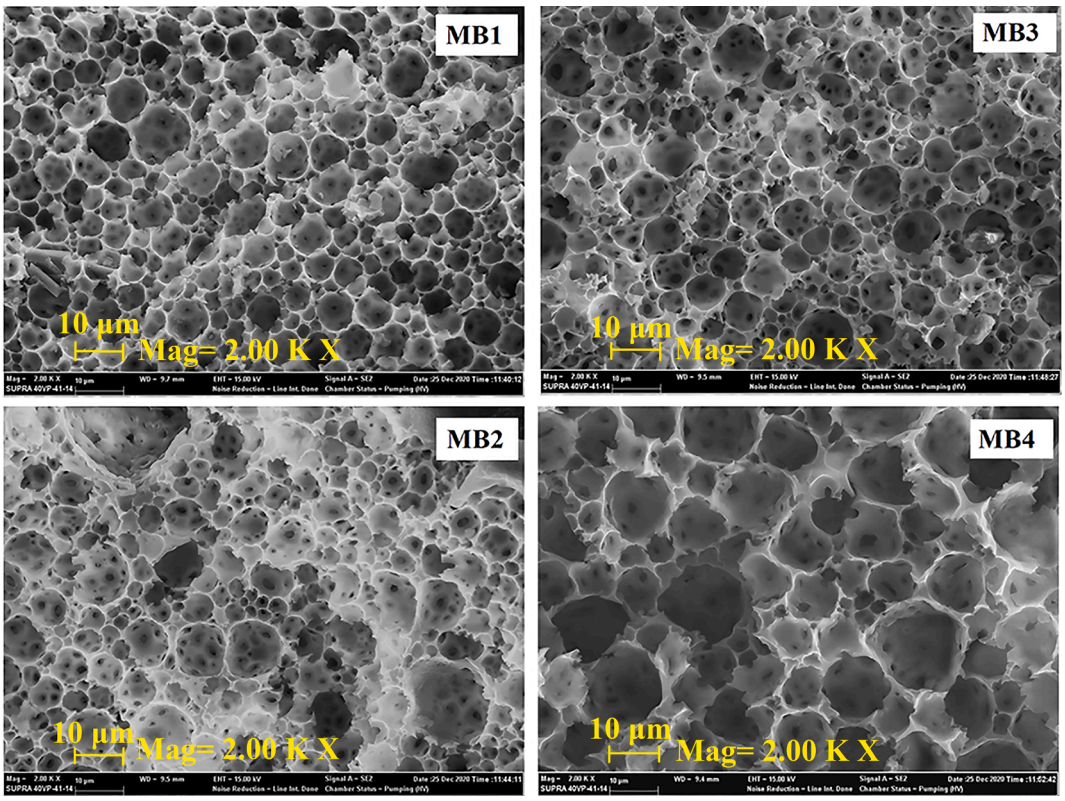

Fig. 1. SEM images of crosslinked polyHIPE samples. (MBx foams; x = 1, 2, 3, 4).

Table 3
Morphological properties of polyHIPEs.

PolyHIPE	CS (µm)	IPS (µm)	δ_{BET} (m^2g^{-1})
MB1	6.51 ± 0.19	0.61 ± 0.02	5.79 ± 0.25
MB2	4.15 ± 0.05	1.23 ± 0.03	3.33 ± 0.18
MB3	7.14 ± 0.20	1.48 ± 0.05	3.11 ± 0.19
MB4	11.70 ± 0.16	1.39 ± 0.04	2.25 ± 0.12
MB9	1.87 ± 0.05	0.12 ± 0.01	36.12 ± 0.23
HMB1	6.38 ± 0.19	0.68 ± 0.02	34.12 ± 1.13
HMB2	7.23 ± 0.31	1.17 ± 0.04	32.86 ± 1.86
HMB3	7.35 ± 0.21	1.27 ± 0.04	39.85 ± 2.04
HMB4	12.76 ± 0.65	1.49 ± 0.05	60.18 ± 3.24
IHMB1	7.59 ± 0.24	0.60 ± 0.02	27.22 ± 0.99
IHMB2	7.81 ± 0.39	1.22 ± 0.03	23.48 ± 0.84
IHMB3	8.10 ± 0.33	1.44 ± 0.04	11.71 ± 0.76
IHMB4	10.77 ± 0.58	1.43 ± 0.05	52.07 ± 2.54

purpose, stress–strain behaviour of the polyHIPE foams (MBx; x = 1, 2, 3, 4) were investigated under uniaxial compressive load. While stress–strain plots are presented in Fig. S2 in the *SI document*, compression modulus (Ec) and compressive stress at 10% deformation (σ_{10}) of the polyHIPE foams are given in Table S1 in the *SI document*. According to the stress–strain plots polyHIPE foams were all exhibited linear elasticity at very low stress values. On the other hand, the shape of stress–strain curves being similar with each other is suggesting the similar deformation mechanisms. As the compression proceeds, foam specimens squeezed with the applied load and the stress was raised with the deformation. It was found that the compressive stress at 10% deformation (σ_{10}) was changed between 979 and 144 kPa (Table S1). This result is demonstrating the relationship between the corresponding polymer matrix of the foams and mechanical properties. Since MB1 foam has also much higher compressive modulus variation of mechanical properties can be attributed to the monomer composition. It can be seen from Fig. S2 and Table S1 that when the amount of BDDA in the monomer mixture decreased mechanical properties of the foams were also regressed and reach the lowest value in foam sample obtained without using BDDA in the monomer mixture (MB4). It can be also noted that when the applied stress was removed each specimen gained the deformation and turned its original dimensions.

In order to improve the specific surface area by using the advantage of monomer composition for future applications, hypercrosslinking was conducted to MB1, MB2, MB3 and MB4 foams. For this purpose, hypercrosslinking procedure was performed either under atmospheric conditions or under Argon atmosphere. Structural characterization of HXL-polyHIPE samples were performed by FTIR analysis. Comparative FTIR spectra of monomers, precursor polyHIPEs (MBx samples; x = 1,2, 3, 4) and HXL-polyHIPEs (HMBx and IHMBx; x = 1,2, 3, 4) were presented in Fig. 2.

It can be seen from the FTIR spectrums presented in Fig. 2(a)–(c) that the characteristic C═O vibration of the ester bond of BDDA is detected at 1728 cm^{-1}. The presence of this peak in the spectrums of MB1, MB2 and MB3 confirms the successful bounding of BDDA units to the polymer chain. On the other hand, detection of this peak also in the spectrums of hypercrosslinked MB1, MB2 and MB3 foams (corresponding HMBx and IHMBx foams) is the second indicator of the formation of copolymer chains containing BDDA units on the polymer sequence. The peaks at 1641 and 811 cm^{-1} in the spectrum of monomer BDDA can be attributed to the C═C stretching of BDDA. Non-existence of these peaks in the spectrums of MB1, MB2 and MB3 and corresponding hypercrosslinked polyHIPEs (HMBx and IHMBx; x = 1, 2, 3) confirms the conversion of double bonds to single bonds with copolymerization. On the other hand, conjugated double bonds of *β*-myrcene are the other decisive in the crosslinking reactions. The peak at 1597 cm^{-1} in the spectrum of β-myrcene can be attributed to the vibrations of the conjugated double bonds [55]. This peak is almost disappeared in the FTIR spectrums of HMBx and IHMBx which could be accepted as the verification of the participation of conjugated double bond in the polymer formation. The peak at 1270 cm^{-1} in the spectrum of VBC can be attributed to the $–CH_2Cl$ group of the monomer [56]. The intensity of this peak is changed

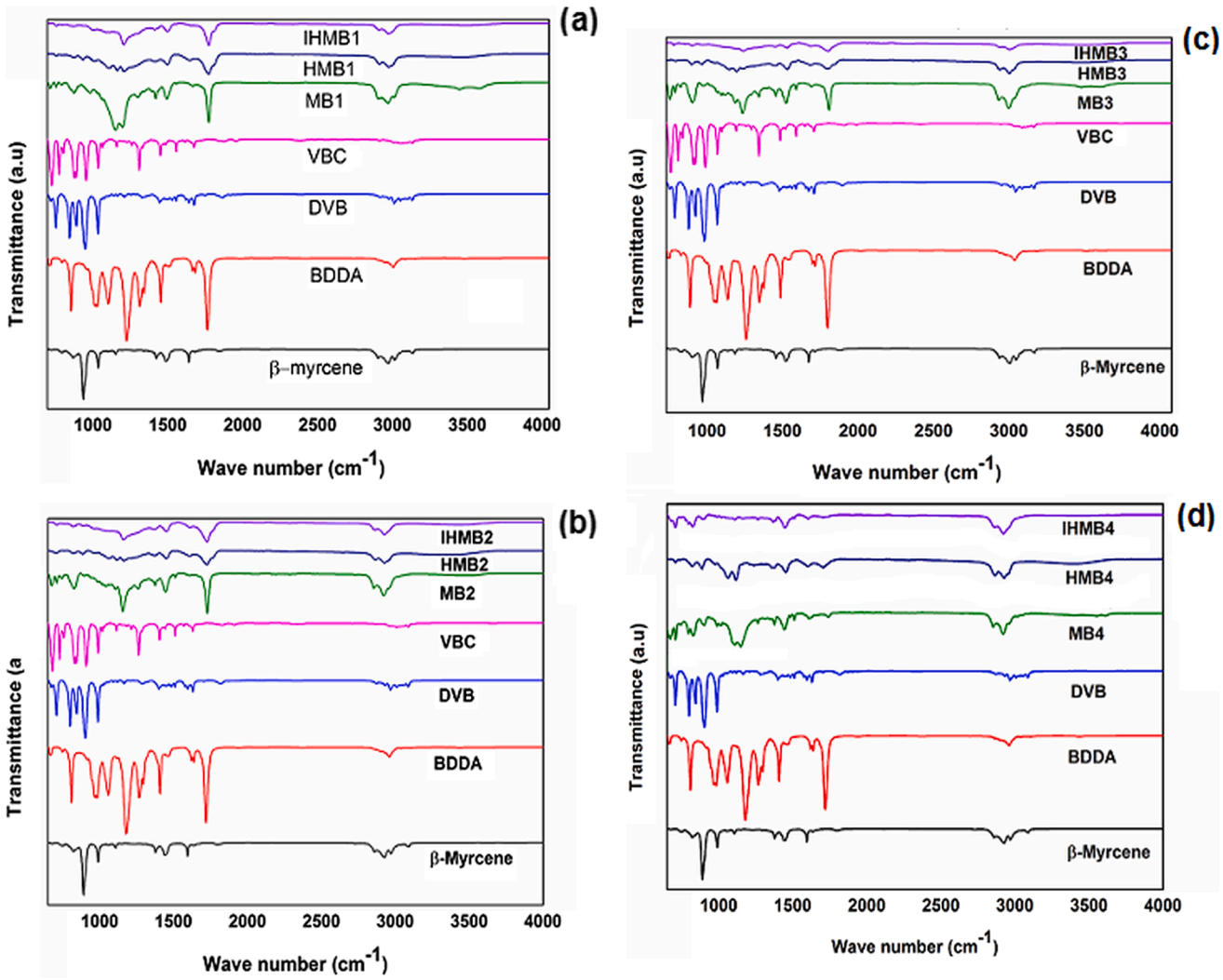

Fig. 2. Comparative FTIR spectra of the monomers (*β*-myrcene, BDDA, DVB and VBC), MBx, HMBx and IHMBx polyHIPEs. (a) MB1, HMB1, and IHMB1, (b) MB2, HMB2, and IHMB2, (c) MB3, HMB3, and IHMB3, (d) MB4, HMB4, and IHMB4.

in the MBx samples, confirms the presence of VBC units on the copolymer chains. In addition, this peak is completely disappeared in the spectrums of HXL-polyHIPEs. The disappearance of this peak in the spectrums of HMBx and IHMBx samples confirms the achievement of hypercrosslinking reactions [41]. In the spectrums of MBx, HMBx and IHMBx samples, the bands appeared between 2800 cm^{-1} and 3100 cm^{-1} is due to the C—H stretches, while the bands appeared at 3000 cm^{-1} belongs to the C—H stretches of the aromatic groups. Moreover, the bands appeared below 3000 cm^{-1} is due to the C—H extensions of alkyl groups of *β*-myrcene and BDDA. In addition to all, the peaks at 700 cm^{-1} and 900 cm^{-1} in the spectrums DVB and VBC can be attributed to the aromatic skeletal bonds. While the intensity of these peaks is slightly declined in MBx samples, they are overlapped in the FTIR spectrums of HMBx and IHMBx.

The variation of chemical structure with hypercrosslinking was also confirmed by ^{1}H NMR characterization by using the crosslinked and HXL-polyHIPE foams prepared from precursor HIPE-3 (MB3, HMB3 and IHMB3). PolyHIPEs obtained from HIPE-3 was used because of its monomer composition composed of 50 vol% of *β*-myrcene, 10 vol% of BDDA, 10 vol% of DVB and 30 vol% of VBC. ^{1}H NMR spectrums of *β*-myrcene, MB3, HMB3 and IHMB3 are presented respectively in Fig. 3 (a)–(d).

Methyl groups which are attached to C8 in all types of microstructures of *β*-myrcene appear at 1.69 and 1.60 ppm (Fig. 3(a)). By copolymerization of *β*-myrcene with other monomers, the signals of these —CH_3 protons disappears and —CH protons of the double bonds appears as a broad peak at the shield between 3.963 and 5.000 in the ^{1}H NMR spectrums of polymers, as in MB3 foam. By hypercrosslinking reaction, this broad peak is shift to upfield and detected at 4.268 ppm in the spectrum of HMB3. When the broad peak of —CH protons observed at 4.268 ppm in the spectrum of HMB3 evaluated with a close look, two splitting at 3.902 and 4.878 ppm are observed, which indicates the presence of other regioregular microstructures of *β*-myrcene. However, this peak appears as a singlet at 4.329 ppm in the spectrum of IHMB3 due to highly hypercrosslinked polymer network. Additionally, the signals of the methylene protons of VBC, aromatic —H of VBC and aromatic —H of DVB are detected at 6.464, 6.830 and 7.807 ppm, respectively in the spectrum of MB3. However, in the spectrum of HMB3, this peak is widened and shifts to the upper field, appears as a single at 8.234 ppm, the same signal cannot be observed in the spectrum of IHMB3. The splitting of the broad peak appear in the magnetic field between 3.963 ppm and 5.00 ppm shows the presence of 3,4- (at 5.00 ppm), 1,4-*cis* and 1,4-*trans* (4.573 and 4.268 ppm), 1,2- microstructure (at 3.963 ppm) of *β*-myrcene in the proton NMR spectrum of MB3. On the other hand, the signal detected at 5.00 ppm due to the presence of 3,4-microstructure is not detected in the spectrum of HMB3. Moreover, the other microstructures of *β*-myrcene such as 1,2-, 1,4-*cis* and 1,4-*trans* also contributed to the polymer network under Argon atmosphere. This

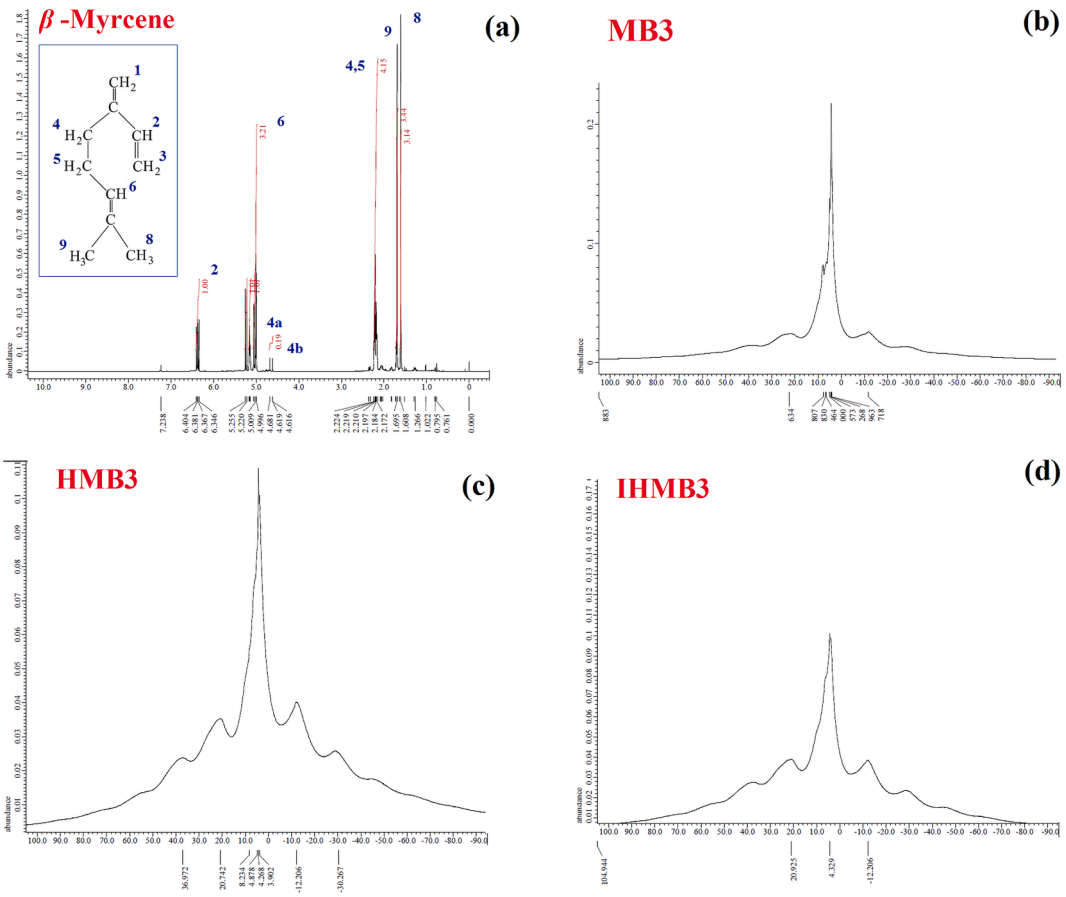

Fig. 3. ^{1}H NMR spectrums of (a) β-myrcene (b) MB3, (c) HMB3 and (d) IHMB3.

contribution is detected by a broad singlet signal at 4.329 ppm. This signal arises due to the presence of variable organic structures in the polymer network [57].

After hypercrosslinking, the morphology of the HXL-polyHIPE samples (HMBx and IHMBx; x = 1, 2, 3, 4) was also investigated with SEM and presented in Fig. 4 in order to reveal the variation of pore structure. Moreover, the comparative change of cavity size distribution after hypercrosslinking was also determined and presented in Fig. 5. As can be seen from Fig. 4, hypercrosslinking did not yield a significant change on the pore structure. In general, average cavity size and interconnected pore size of the hypercrosslinked samples (HMBx and IHMBx) were found to be similar with those the corresponding MBx samples. In addition to all, it was determined that atmospheric conditions during the hypercrosslinking reaction did not have a considerable importance. Reactions conducted at the inert atmosphere resulted similar variation of pore structure with the ones conducted at normal conditions. By comparing the cavity size distribution of MBx samples with the cavity size distributions of HMBx and IHMBx samples, it was determined that hypercrosslinking did not cause a significant change on cavity size distribution (Fig. 5).

On the other hand, specific surface area of the HMBx and IHMBx samples were also determined right after hypercrosslinking reactions and the results were presented in Table 3. Despite that hypercrosslinking caused only an insignificant change in pore structure, a remarkable change was observed for specific surface area of the obtained polyHIPEs. As can be seen from Table 3, while the specific surface area of the MBx samples (x = 1, 2, 3 and 4) was changing in the range between 5.79 m^2g^{-1} and 2.25 m^2g^{-1}, it was changing between 34.12 m^2g^{-1} and 60.18 m^2g^{-1}, 27.22 m^2g^{-1} and 52.07 m^2g^{-1}, respectively for HMBx and IHMBx samples. According to this results, higher increase in specific surface area was observed for the polyHIPE sample which was prepared by using 25 vol% of VBC monomer in the monomer composition. However, the improvement in the specific surface area was unfortunately not as high as the previously published results [58,59]. This result can be attributed to the monomer composition of the precursor HIPEs. Since crosslinked polyHIPE foams cannot be obtained using large amounts of VBC in the HIPE formulation, the formation of methylene bridges between neighboring molecules is limited [40,60].

4. Conclusion

PolyHIPEs are an important class of hierarchical macroporous polymer foams. In recent years, they have become important candidates especially for the storage of gases, liquids and energy, due to their unique morphology and ease of preparation. Thereby, developing a bio-based sustainable polyHIPE is an important goal. In the scientific literature there is limited number of studies focused on the copolymerization of terpene derives within HIPE templates.

In this study, we prepared macroporous polyHIPEs from w/o type HIPEs consisting β-myrcene in the continuous phase. β-Myrcene is a linear conjugated dien and an important acyclic monoterpene derivate. Because it is commercially available, cost effective, and provides chemistry similar with hydrocarbons there is a growing interest on implementing this terpene in the synthesis of sustainable polymers. Moreover, when β-myrcene is polymerized it provides polyisoprene like chain structure and leads the formation of rubbery polymers. Within this context, we prepared HIPEs in which the volume fraction of β-myrcene was either 40 or 50% in the monomer mixture. We also investigated the copolymerization crosslinking performance of β-myrcene based HIPEs in the presence of BDDA, VBC, and DVB comonomers by altering the comonomer amounts between 0 and 60 vol% of the monomer mixture. Accordingly, the influence of monomer composition on the emulsion

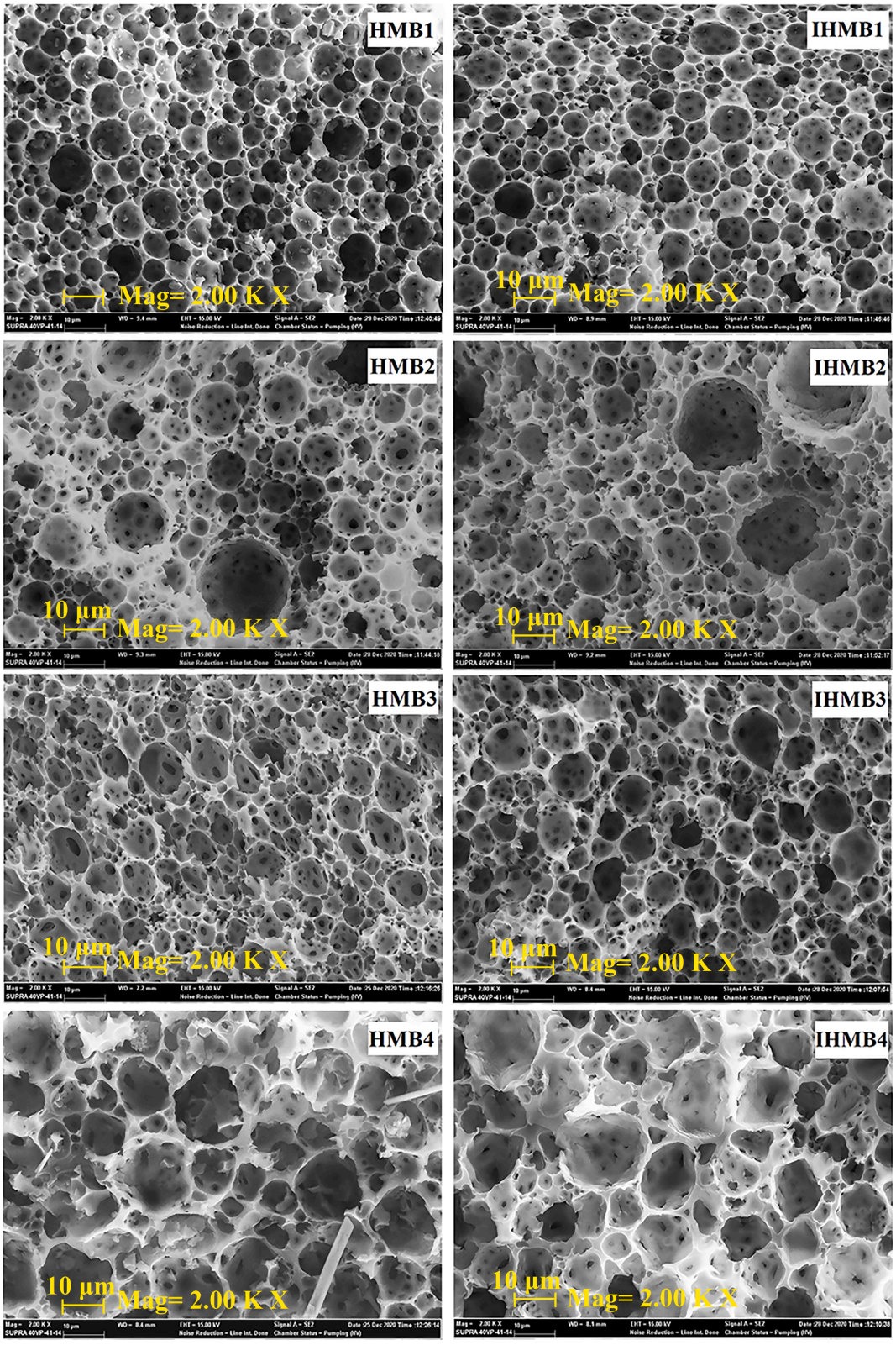

Fig. 4. SEM images of HXL-polyHIPE foams (HMBx and IHMBx foams; x = 1, 2, 3, 4).

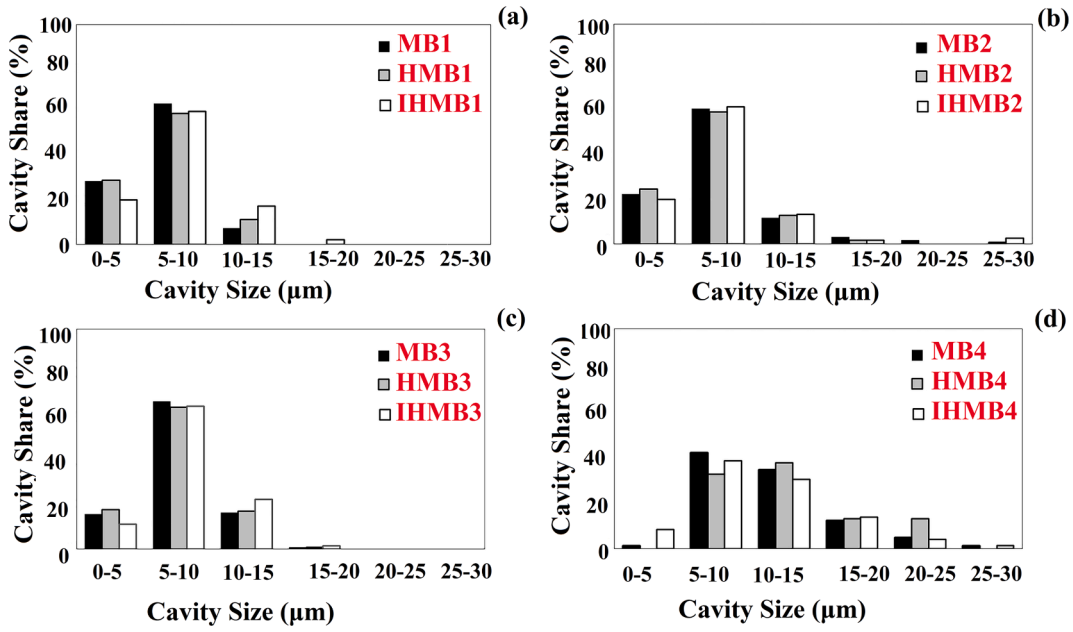

Fig. 5. Comparative cavity size distribution graphs of MBx, HMBx, and IHMBx foams: (a) MB1, HMB1, and IHMB1, (b) MB2, HMB2, and IHMB2, (c) MB3, HMB3, and IHMB3, (d) MB4, HMB4, and IHMB4.

stability and polyHIPE morphology were also demonstrated. It was shown that monomer composition has a great influence on the formation of crosslinked polymyrcene network. Thanks to the functionality of the comonomers, we also achieved to create suitable sites for post-polymerization hypecrosslinking by Friedel-Crafts alkylation. Although the resulting polyHIPE foams exhibited very low specific surface areas, we achieved to increase the BET specific surface area of the polyHIPEs up to 60 m^2g^{-1} by hypercrosslinking. Nevertheless, we also showed that a deeper understanding of the copolymerization kinetics of this terpene derivative is required to enable the development of fully bio-based polyHIPEs. We believe that terpene based polyHIPE foams will be good candidates for the preparation of polymer-supported phase change materials (PCMs).

5. Data availability

The data that support the findings of this study are available from the authors, upon reasonable request.

Declaration of Competing Interest

The authors declare that they have no known competing financial interests or personal relationships that could have appeared to influence the work reported in this paper.

Appendix A. Supplementary material

Supplementary data to this article can be found online at https://doi.org/10.1016/j.eurpolymj.2021.110474.

References

[1] N. Barlık, B. Keskinler, M.M. Kocakerim, G. Akay, Surface modification of monolithic PolyHIPE Polymers for anionic functionality and their ion exchange behavior, J. Appl. Polym. Sci. 132 (2015) 42286, https://doi.org/10.1002/app.42286.
[2] C. Zhao, E. Danish, N.R. Cameron, R. Kataky, Emulsion-templated porous materials (PolyHIPEs) for selective ion and molecular recognition and transport: applications in electrochemical sensing, J. Mater. Chem. 17 (2007) 2446–2453, https://doi.org/10.1039/B700929A.
[3] V.Ş. Ünnü, S. Çetinkaya, Synthesis and Catalytic Activity of polyHIPE-supported NHCbearing ruthenium initiator for ROMP, Catal. Lett. 148 (2018) 2432–2445, https://doi.org/10.1007/s10562-018-2467-4.
[4] R. Mravljak, O. Bizjak, B. Božič, M. Podlogar, A. Podgornik, Flow-through polyHIPE silver-based catalytic reactor, Polymers 13 (2021) 880, https://doi.org/10.3390/polym13060880.
[5] H.H. Mert, PolyHIPE composite based form stable phase change material for thermal energy storage, Int. J. Energy Res. 44 (2020) 6583–6594, https://doi.org/10.1002/er.5390.
[6] A.B. Deshmukh, A.C. Nalawade, I. Karbhal, M.S. Qureshi, M.V. Shelke, Electrochemical capacitive energy storage in PolyHIPE derived nitrogen enriched hierarchical porous carbon nanosheets, Carbon 128 (2018) 287–295, https://doi.org/10.1016/j.carbon.2017.11.080.
[7] M.S. Silverstein, N.R. Cameron, PolyHIPEs — Porous polymers from high internal phase emulsions. Encyclopedia of Polymer Science and Technology, John Wiley & Sons, Inc., New York, 2010.
[8] M.S. Silverstein, PolyHIPEs: Recent advances in emulsion-templated porous polymers, Prog. Polym. Sci. 39 (2014) 199–234, https://doi.org/10.1016/j.progpolymsci.2013.07.003.
[9] N.R. Cameron, D.C. Sherrington, High internal phase emulsions (HIPEs) — Structure, properties and use in polymer preparation, in: B.L.C.P.P. Emulsion (Ed.), Advances in Polymer Science, Heidelberg, Springer, Berlin, 1996, pp. 163–214.
[10] H.H. Mert, M.S. Mert, E.H. Mert, A statistical approach for tailoring the morphological and mechanical properties of polystyrene PolyHIPEs: looking through experimental design, Mater. Res. Express. 6 (2019), 115306, https://doi.org/10.1088/2053-1591/ab437f.
[11] E.H. Mert, H.H. Mert, Preparation of polyHIPE nanocomposites: Revealing the influence of experimental parameters with the help of experimental design approach, Polym. Compos. 42 (2021) 724–738, https://doi.org/10.1002/pc.25861.
[12] N.R. Cameron, High internal phase emulsion templating as a route to well-defined porous polymers, Polymer 46 (2005) 1439–1449, https://doi.org/10.1016/j.polymer.2004.11.097.
[13] I. Pulko, J. Wall, P. Krajnc, N.R. Cameron, Ultra-high surface area functional porous polymers by emulsion templating and hypercrosslinking: efficient nucleophilic catalyst supports, Chem. Eur. J. 16 (2010) 2350–2354, https://doi.org/10.1002/chem.200903043.
[14] J.H. Ahn, J.E. Jang, C.G. Oh, S.K. Ihm, J. Cortez, D.C. Sherrington, Rapid generation and control of microporosity, bimodal pore size distribution, and surface area in davankov-type hyper-cross-linked resins, Macromolecules 39 (2006) 627–632, https://doi.org/10.1021/ma051152n.
[15] V.A. Davankov, V.A. Tsyurupa, Structure and properties of hypercrosslinked polystyrene—the first representative of a new class of polymer networks, React. Polym. 13 (1990) 27–42, https://doi.org/10.1016/0923-1137(90)90038-6.
[16] V. Pastukhov, M.P. Tsyurupa, V.A. Davankov, Hypercrosslinked polystyrene: A polymer in a non-classical physical state, J. Polym. Sci. Pt B Polym. Phys. 37 (1999) 2324–2333, https://doi.org/10.1002/(SICI)1099-0488(19990901)37:17<2324::AID-POLB4>3.0.CO;2-B.
[17] P. Veverka, K. Jeřábek, Mechanism of hypercrosslinking of chloromethylated styrene–divinylbenzene copolymers, React. Funct. Polym. 41 (1999) 21–25, https://doi.org/10.1016/S1381-5148(99)00030-9.

[18] M.P. Tsyurupa, V.A. Davankov, Hypercrosslinked polymers: basic principle of preparing the new class of polymeric materials, React. Funct. Polym. 53 (2002) 193–203, https://doi.org/10.1016/S1381-5148(02)00173-6.
[19] P. Veverka, K. Jeřábek, Influence of hypercrosslinking on adsorption and absorption on or in styrenic polymers, React. Funct. Polym. 59 (2004) 71–79, https://doi.org/10.1016/j.reactfunctpolym.2003.12.008.
[20] D. Wang, N.L. Smith, P.M. Budd, Polymerization and carbonization of high internal phase emulsions, Polym. Int. 54 (2005) 297–303, https://doi.org/10.1002/pi.1672.
[21] F.S. Macintyre, D.C. Sherrington, L. Tetley, Synthesis of ultrahigh surface area monodisperse porous polymer nanospheres, Macromolecules 39 (2006) 5381–5384, https://doi.org/10.1021/ma0610010.
[22] R.T. Woodward, A. Jobbe-Duval, S. Marchesini, D.B. Anthony, C. Petit, A. Bismarck, Hypercrosslinked polyHIPEs as precursors to designable, hierarchically porous carbon foams, Polymer 115 (2017) 146–153, https://doi.org/10.1016/j.polymer.2017.03.042.
[23] S. Huš, P. Krajnc, PolyHIPEs from methyl methacrylate: Hierarchically structured microcellular polymers with exceptional mechanical properties, Polymer 55 (2014) 4420–4424, https://doi.org/10.1016/j.polymer.2014.07.007.
[24] A. Barbetta, M. Dentini, L. Leandri, G. Ferraris, A. Coletta, M. Bernabei, Synthesis and characterization of porous glycidylmethacrylate–divinylbenzene monoliths using the high internal phase emulsion approach, React. Func. Polym. 69 (2009) 724–736, https://doi.org/10.1016/j.reactfunctpolym.2009.05.007.
[25] S. Mezhouda, M. Paljevac, A. Koler, B.L. Droumaguet, D. Grande, P. Krajnc, Novel hypercrosslinking approach toward high surface area functional 2-hydroxyethyl methacrylate-based polyHIPEs, React. Func. Polym. 132 (2018) 51–59, https://doi.org/10.1016/j.reactfunctpolym.2018.09.009.
[26] N.R. Cameron, D.C. Sherrington, Preparation and glass transition temperatures of elastomeric PolyHIPE materials, J. Mater. Chem. 7 (1997) 2209–2212, https://doi.org/10.1039/A702030I.
[27] S. Kovačič, C. Slugovc, Ring-opening Metathesis Polymerisation derived poly (dicyclopentadiene) based materials, Mater. Chem. Front. 4 (2020) 2235–2255, https://doi.org/10.1039/D0QM00296H.
[28] M.G. Pérez-García, M.C. Gutierrez, J.D. Mota-Morales, G. Luna-Barcenas, F. del Monte, Synthesis of biodegradable macroporous poly(L-lactide)/ poly (ε-caprolactone) blend using oil-in-eutectic-mixture high internal phase emulsions as template, ACS Appl. Mater. Interfaces 8 (2016) 16939–16949, https://doi.org/10.1021/acsami.6b04830.
[29] C. Chen, A.M. Eissa, T.L. Schiller, N.R. Cameron, Emulsion-templated porous polymers prepared by thiol-ene and thiol-yne photopolymerisation using multifunctional acrylate and non-acrylate monomers, Polymer 126 (2017) 395–401, https://doi.org/10.1016/j.polymer.2017.04.021.
[30] B. Sergent, M. Birot, H. Deleuze, Preparation of thiol–ene porous polymers by emulsion templating, React. Funct. Polym. 72 (2012) 962–966, https://doi.org/10.1016/j.reactfunctpolym.2012.02.011.
[31] E. Berber, F. Çira, E.H. Mert, Preparation of porous polyester composites via emulsion templating: Investigation of the morphological, mechanical, and thermal properties, Polym. Compos. 37 (2016) 1531–1538, https://doi.org/10.1002/pc.23323.
[32] E.H. Mert, M.A. Kaya, H. Yıldırım, Preparation and Characterization of Polyester-Glycidyl Methacrylate PolyHIPE Monoliths to Use in Heavy Metal Removal, Des. Monomers Polym. 15 (2012) 113–126, https://doi.org/10.1163/156855511X615001.
[33] P. Steindl, H. Decker, B. Retzl, Q. Jiang, A. Menner, A. Bismarck, Emulsion-templated flexible epoxy foams, Polymer (2021), 123380, https://doi.org/10.1016/j.polymer.2021.123380.
[34] A. Szczurek, V. Fierro, M. Thébault, A. Pizzi, A. Celzard, Structure and properties of poly(furfuryl alcohol)-tannin polyHIPEs, Eur. Polym. J. 78 (2016) 195–212, https://doi.org/10.1016/j.eurpolymj.2016.03.037.
[35] A. Matic, H. Schlaad, Thiol-ene photofunctionalization of 1,4-polymyrcene, Polym. Int. 67 (2018) 500–505, https://doi.org/10.1002/pi.5534.
[36] A. Behr, L. Johnen, Myrcene as a natural base chemical in sustainable chemistry: A critical review, Chem. Sus. Chem. 2 (2009) 1072–1095, https://doi.org/10.1002/cssc.200900186.
[37] P. Sahu, P. Sarkar, A.K. Bhowmick, Design of a molecular architecture via a green route for improved silica reinforced nanocomposite using bio-resources, ACS Sustainable Chem. Eng. 6 (2018) 6599–6611, https://doi.org/10.1021/acssuschemeng.8b00383.
[38] T. Nishida, K. Satoh, M. Kamigaito, Biobased polymers via radical homopolymerization and copolymerization of a series of terpenoid-derived conjugated dienes with exo-methylene and 6-membered ring, Molecules 25 (2020) 5890, https://doi.org/10.3390/molecules25245890.
[39] E.H. Mert, B. Kekevi, Synthesis of polyHIPEs through high internal phase emulsions of β-myrcene, Colloid Polym. Sci. 298 (2020) 1423–1432, https://doi.org/10.1007/s00396-020-04730-4.
[40] A. Koler, P. Krajnc, Surface modification of hypercrosslinked vinylbenzyl chloride polyHIPEs by grafting via RAFT, Macromol. Chem. Phys. 222 (2021) 2000381, https://doi.org/10.1002/macp.202000381.
[41] R. Castaldo, R. Avolio, M. Cocca, G. Gentile, M.E. Errico, M. Avella, C. Carfagna, V. Ambrogi, A Versatile synthetic approach toward hyper-cross-linked styrene based polymers and nanocomposites, Macromolecules 50 (2017) 4132–4143, https://doi.org/10.1021/acs.macromol.7b00812.
[42] A. Barbetta, N.R. Cameron, Morphology and surface area of emulsion-derived (polyhipe) solid foams prepared with oil-phase soluble porogenic solvents: span 80 as surfactant, Macromolecules 37 (2004) 3188–3201, https://doi.org/10.1021/ma0359436.
[43] J. Park, K. Kim, M. Seo, Hyper-cross-linked polymer with controlled multiscale porosity via polymerization-induced microphase separation within high internal phase emulsion, Chem. Commun. 54 (2018) 7908–7911, https://doi.org/10.1039/C8CC03508C.
[44] D.L. Trumbo, Free radical copolymerization behavior of myrcene I. Copolymers with styrene, methyl methacrylate or p-fluorostyrene, Polym. Bulletin 31 (1993) 629–636. https://doi.org/10.1007/BF00300120.
[45] A.C. Weems, K.R. Delle Chiaie, R. Yee, A.P. Dove, Selective reactivity of myrcene for vat photopolymerization 3d printing and post fabrication surface modification, Biomacromolecules 21 (2020) 163–170, https://doi.org/10.1021/acs.biomac.9b01125.
[46] P. Sarkar, A.K. Bhowmick, A Green approach towards sustainable polymer: synthesis and characterization of poly(myrcene-co-dibutyl itaconate), ACS Sustainable Chem. Eng. 4 (2016) 2129–2141, https://doi.org/10.1021/acssuschemeng.5b01591.
[47] P. Taylor, Ostwald ripening in emulsions, Colloids Surf. A: Physicochem. Eng. Aspects 99 (1995) 175–185, https://doi.org/10.1016/0927-7757(95)03161-6.
[48] A.S. Kabalnov, E.D. Shchukin, Ostwald Ripening Theory: Applications to fluorocarbon Emulsion Stability, Adv. Colloid Interface Sci. 38 (1992) 69–97, https://doi.org/10.1016/0001-8686(92)80043-W.
[49] A. Barbetta, N.R. Cameron, S.J. Cooper, High internal phase emulsions (HIPEs) containing divinylbenzene and 4-vinylbenzyl chloride and the morphology of the resulting PolyHIPE materials, Chem. Commun. 3 (2000) 221–222, https://doi.org/10.1039/A909060F.
[50] N. Bauer, J. Brunke, G. Kali, Controlled radical polymerization of myrcene in bulk: Mapping the effect of conditions on the system, ACS Sustainable Chem. Eng. 5 (2017) 10084–10092, https://doi.org/10.1021/acssuschemeng.7b02091.
[51] R.J. Orr, H.L. Williams, The polymerization of isoprene and 2,3-dimethylbutadiene and copolymerization with styrene at −18 °C in emulsion, Can. J. Chem. 30 (1952) 108–123, https://doi.org/10.1139/v52-016.
[52] G. Moad, Reversible addition-fragmentation chain transfer (co)polymerization of conjugated diene monomers: Butadiene isoprene and chloroprene, Polym. Int. 66 (2017) 26–41, https://doi.org/10.1002/pi.5173.
[53] J. Asua, Polymer Reaction Engineering, Blackwell Publishing, 2007. ISBN: 978-1-4051-4442-1.
[54] M.R. Krishnan, Y.F. Aldawsari, E.H. Alsharaeh, Three-Dimensionally cross-linked styrene-methyl metacrylate-divinyl benzene terpolymer networks for organic solvents and crude oil absorption, J. Appl. Polym. Sci. 138 (2021) 49942, https://doi.org/10.1002/app.49942.
[55] P. Sarkar, A.K. Bhowmick, Synthesis, characterization and properties of a bio-based elastomer: Polymyrcene, RSC Adv. 4 (2014) 61343–61354, https://doi.org/10.1039/C4RA09475A.
[56] J.J. Mannion, T.S. Wang, An infrared study of the CH_2Cl group in benzyl chloride and derivatives, Spectrochim. Acta 20 (1964) 45–49, https://doi.org/10.1016/0371-1951(64)80199-5.
[57] P. Sahu, A.K. Bhowmick, Sustainable self-healing elastomers with thermo reversible network derived from biomass via emulsion polymerization, J. Polym. Sci. Part A: Polym. Chem. 57 (2019) 738–751, https://doi.org/10.1002/pola.29320.
[58] Y. Zhang, Y. Li, F. Wang, Y. Zhao, C. Zhang, X. Wang, J.X. Jiang, Hypercrosslinked microporous organic polymer networks derived from silole-containing building blocks, Polymer 55 (2014) 5746–5750, https://doi.org/10.1016/j.polymer.2014.09.014.
[59] N. Fontanals, M. Galia, P.A.G. Cormack, R.M. Marce, D.C. Sherrington, F. Borrull, Evaluation of a new hypercrosslinked polymer as a sorbent for solid-phase extraction of polar compounds, J. Chromatogr. A 1075 (2005) 51–56, https://doi.org/10.1016/j.chroma.2005.04.010.
[60] L. Tan, B. Tan, Hypercrosslinked porous polymer materials: design, synthesis, and applications, Chem. Soc. Rev. 46 (2017) 3322–3356, https://doi.org/10.1039/C6CS00851H.